actuators

MDPI

Article

Optimizing High-Power Performance of [001]-Oriented $Pb(Mg_{1/3}Nb_{2/3})$-$PbTiO_3$ Through Combined DC and AC Polarization Above Curie Temperature

Yuliang Zhu, Xiaobo Wang, Wenchao Xue, Xinran Wen and Chengtao Luo *

School of Electronic Information and Electrical Engineering, Shanghai Jiao Tong University, Shanghai 200240, China; zhuyl2@sjtu.edu.cn (Y.Z.); 022035910015@sjtu.edu.cn (X.W.); wenchao.xue@sjtu.edu.cn (W.X.); spriter@sjtu.edu.cn (X.W.)
* Correspondence: cluo1989@sjtu.edu.cn

Abstract: $Pb(Mg_{1/3}Nb_{2/3})O_3$-$PbTiO_3$ single crystals (PMN-PT SCs) are widely utilized in high-performance piezoelectric devices due to their exceptional piezoelectric properties. Among the various post-processing techniques for domain engineering in PMN-PT SCs, alternating current polarization (ACP) has become a widely adopted method for enhancing piezoelectric performance. This study proposes a new ultrahigh-temperature field-cooling polarization (UFCP) technique, combining direct current polarization (DCP) and ACP with field cooling above the Curie temperature. Dielectric spectra indicate that the UFCP method promotes electric field-induced phase transitions above the Curie point, forming a stable multiphase configuration. The transverse piezoelectric coefficient d_{31} of UFCP SCs is 1126 pC/N, and the electromechanical coupling factor k_{31} is 0.559. Compared with traditional DCP, UFCP increases d_{31} by 68.6%, the mechanical quality factor Q_m by 16.7%, and the piezoelectric figure of merit (FOM) by 98.3%. Furthermore, under high-power excitation with a root-mean-square voltage of 15 V, UFCP achieves a 343% increase in power and a 130.5% improvement in the FOM compared with DCP, demonstrating its potential for enhancing high-power performance in practical applications.

Keywords: PMN-PT; piezoelectric; alternating current polarization (ACP); ultrahigh-temperature field-cooling polarization (UFCP); field cooling; high power; Curie temperature

Academic Editor: Jose Luis Sanchez-Rojas

Received: 29 December 2024
Revised: 20 January 2025
Accepted: 22 January 2025
Published: 24 January 2025

Citation: Zhu, Y.; Wang, X.; Xue, W.; Wen, X.; Luo, C. Optimizing High-Power Performance of [001]-Oriented $Pb(Mg_{1/3}Nb_{2/3})$-$PbTiO_3$ Through Combined DC and AC Polarization Above Curie Temperature. *Actuators* **2025**, *14*, 53. https://doi.org/10.3390/act14020053

1. Introduction

High-performance piezoelectric materials are extensively used in sensors, actuators, transducers, and micro-electromechanical systems (MEMSs) due to their ability to enable efficient bidirectional conversion between mechanical and electrical energy [1–4]. The increasing demand for high-power piezoelectric devices, such as ultrasonic motors and transducers, has driven research toward improving material performance under high-voltage conditions [5–7]. Advancing piezoelectric materials with concurrently enhanced piezoelectric coefficient d and mechanical quality factor Q_m remains a central challenge and focus in the field, as these parameters are critical to achieving high energy conversion efficiency and low energy dissipation [8,9]. Despite progress, mainstream piezoelectric materials like $Pb(Zr_{1-x}Ti_x)O_3$ (PZT) remain limited by low performance, highlighting the need for advanced materials with improved properties [4,10].

Relaxor-ferroelectric single crystals (SCs), exemplified by $Pb(Mg_{1/3}Nb_{2/3})O_3$-$PbTiO_3$ (PMN-PT), have garnered remarkable attention due to their exceptional piezoelectric coefficient ($d_{33} > 2000$ pC/N) and outstanding electromechanical coupling factor

($k_{33} > 90\%$) [11,12], especially when the lead titanate ($PbTiO_3$, PT) content approaches the morphotropic phase boundary (MPB) [13,14]. However, the relatively low Q_m of PMN-PT SCs poses a challenge, as it reduces energy transfer efficiency and device durability, thereby limiting their applicability in high-power piezoelectric systems [15].

To enhance the performance of PMN-PT SCs, researchers have proposed various strategies, including exploring solid-solution systems [9] and modulating lattice defects through doping [16]. However, the associated low efficiency and high cost constrain their feasibility for large-scale applications. In recent years, domain engineering has emerged as a straightforward and cost-effective approach to optimize functional properties by precisely manipulating domain structures without altering material composition [17,18]. Since Yamashita et al. introduced alternating current polarization (ACP) into PMN-PT SCs and noticeably improved the piezoelectric and dielectric properties, ACP has gained considerable attention and application among various domain engineering methods [19]. Over the past years, extensive research has been conducted on the influence of crystal orientation [20,21], composition [22,23], poling temperature [24,25], and electric field [18,26] on the effectiveness of ACP. Compared with traditional direct current polarization (DCP), ACP has been shown to induce monoclinic (M) phase formation [21], fulfill long-range order [18], and refine domain configuration [27], leading to substantial improvements in piezoelectric performance. In addition to ACP, the field-cooling polarization (FCP) method has also been extensively studied in recent years [28–31]. For MPB-region PMN-PT SCs, two distinct phase transitions are typically observed before reaching the Curie temperature (T_C): the transition from the rhombohedral (R) phase to the M phase (T_{d1}) and subsequently from the M phase to the tetragonal (T) phase (T_{d2}) [21]. During conventional FCP, piezoelectric samples are heated near the first phase transition temperature (T_{d1}) and then subjected to a constant DC field while cooling [28]. Luo et al. combined ACP and FCP, applying ACP at a high temperature ($90\ ^\circ C > T_{d1}$) of relaxor ferroelectrics. This hybrid approach leveraged multiphase transitions to induce monoclinic phases, effectively improving the piezoelectric properties [29]. Furthermore, Shibiru et al. pioneered combining AC-DC poling at ultrahigh temperatures in barium titanate ($BaTiO_3$) ceramics, precisely above T_C. This method successfully formed finer domain structures, leading to remarkable enhancements in piezoelectric performance [30,31]. Despite these advancements, the effects of ultrahigh-temperature polarization on relaxor ferroelectrics such as PMN-PT remain unexplored, and the suitability of ACP in FCP applications warrants further exploration.

Piezoelectric materials with high Q_m exhibit minimal energy dissipation, rendering them ideal candidates for power piezoelectric devices [32,33]. However, most reported measurements of Q_m are derived from the small-signal method, typically using low voltage levels, such as 1Vpp. These measurements cannot be directly extrapolated to the design of high-power devices. This limitation arises because piezoelectric materials exhibit pronounced nonlinear behavior under strong electric fields, with performance parameters varying with field strength [34,35]. To address the limitation, performing precise characterizations of piezoelectric materials under high-voltage driving conditions is crucial. For instance, Li et al. conducted comparative studies on the performance of PZT-4 and $Pb(In_{1/2}Nb_{1/2})O_3$-$Pb(Mg_{1/3}Nb_{2/3})O_3$-$PbTiO_3$ (PIN-PMN-PT) under high driving voltage [36]. Zheng et al. explored the behavior of PMN-PT 1-3 composites under high electric field [5]. Despite these advancements, systematic studies on the impact of domain engineering techniques on the high-power performance of piezoelectric materials remain scarce. This lack of research hinders ACP's broader application and development in power piezoelectric devices [37].

In this study, we propose and validate an innovative ultrahigh-temperature field-cooling polarization (UFCP) method, which integrates DCP and ACP processes with FCP

above T_C to optimize the polarization of [001]-oriented PMN-0.30PT SCs. The UFCP PMN-PT SCs were comprehensively evaluated by using conventional small-signal characterization methods and high-power piezoelectric performance assessment techniques. The dielectric spectrum revealed that the enhancement in piezoelectric performance is closely associated with the formation of multiphase domain structures induced by electric field-driven phase transitions near T_C. UFCP demonstrated significant improvements in the high-power piezoelectric performance of PMN-PT SCs, offering a new approach and scientific foundation for their practical application under high-electric field conditions.

2. Experimental Details

The high-quality PMN-0.30PT SCs used in this study were grown by using a modified Bridgman method by the Shanghai Institute of Ceramics, Chinese Academy of Sciences [38]. The PMN-PT SCs were fabricated in length vibration mode and precisely cut and polished to dimensions of $16 \times 4 \times 0.8$ mm^3, with the length, width, and thickness aligned along the $[100]_c$, $[010]_c$, and $[001]_c$ crystallographic directions, respectively. The electrode surfaces made of silver conductive paste were oriented perpendicular to the $[001]_c$ direction, which also served as the polarization axis. Four samples were tested to ensure experimental reproducibility, and each sample underwent multiple polarization treatments under various conditions. Before each polarization procedure, the samples were heated to 250 °C with shorted top and bottom electrodes for 30 min to ensure complete depolarization.

This study systematically compared six distinct polarization methods, differentiated by the thermal and electric field histories during the polarization process, as illustrated in Figure 1. All polarization processes were conducted in an oil bath to ensure safety during high-voltage operations. The required electric field signals were generated by using a function generator (Textronix AFG1022, Tektronix, Beaverton, OR, USA) and amplified with a high-voltage amplifier (Aigtek ATA-7050, Aigtek, Xi'an, China). The polarization temperatures T_P included 135 °C (above T_C), 70 °C (near T_{d1}), and 25°C (room temperature, RT), representing different thermal conditions for field-cooling polarization. Two types of electric fields were employed. For DCP samples, a DC field of 7.5 kV/cm (3–4 times the coercive field, E_c) was applied for 5 min at the target temperature (IEEE standards [39]), and the samples were subsequently cooled to RT while maintaining the applied DC field. For DCP-ACP combined samples, a symmetric triangular wave field with a frequency of 0.1 Hz and a peak intensity of 15 kVpp/cm was applied for 10 cycles, followed by a 7.5 kV/cm DC field for 5 min. The samples were subsequently cooled to RT while maintaining the DC electric field.

The small-signal characteristics of the PMN-PT samples were measured following IEEE standards [40]. The longitudinal piezoelectric coefficient (d_{33}) was measured by using a quasistatic piezo meter (ZJ-6BN type, Chinese Academy of Science, Beijing, China). The temperature dependence of the free dielectric constant ($\varepsilon_{33}^T/\varepsilon_0$) and dielectric loss (tanδ) were measured at 1kHz by using an impedance analyzer (Agilent 4294A, Agilent, Santa Clara, CA, USA). The impedance spectra under small-signal excitation were obtained at RT (25 °C) by using the impedance analyzer. Key parameters such as the electromechanical coupling factor (k_{31}), elastic compliance (s_{11}^E), and transverse piezoelectric coefficient (d_{31}) were calculated from the resonance and anti-resonance frequencies (f_r and f_a) based on the following equations:

$$\frac{k_{31}^2}{1-k_{31}^2} = \frac{\pi}{2}\frac{f_a}{f_r}\tan\left(\frac{\pi}{2}\frac{f_a-f_r}{f_r}\right) \quad (1)$$

$$s_{11}^E = \frac{1}{4\rho l^2 f_r^2} \quad (2)$$

$$d_{31} = k_{31}\sqrt{\varepsilon_{33}^{T} s_{11}^{T}}. \quad (3)$$

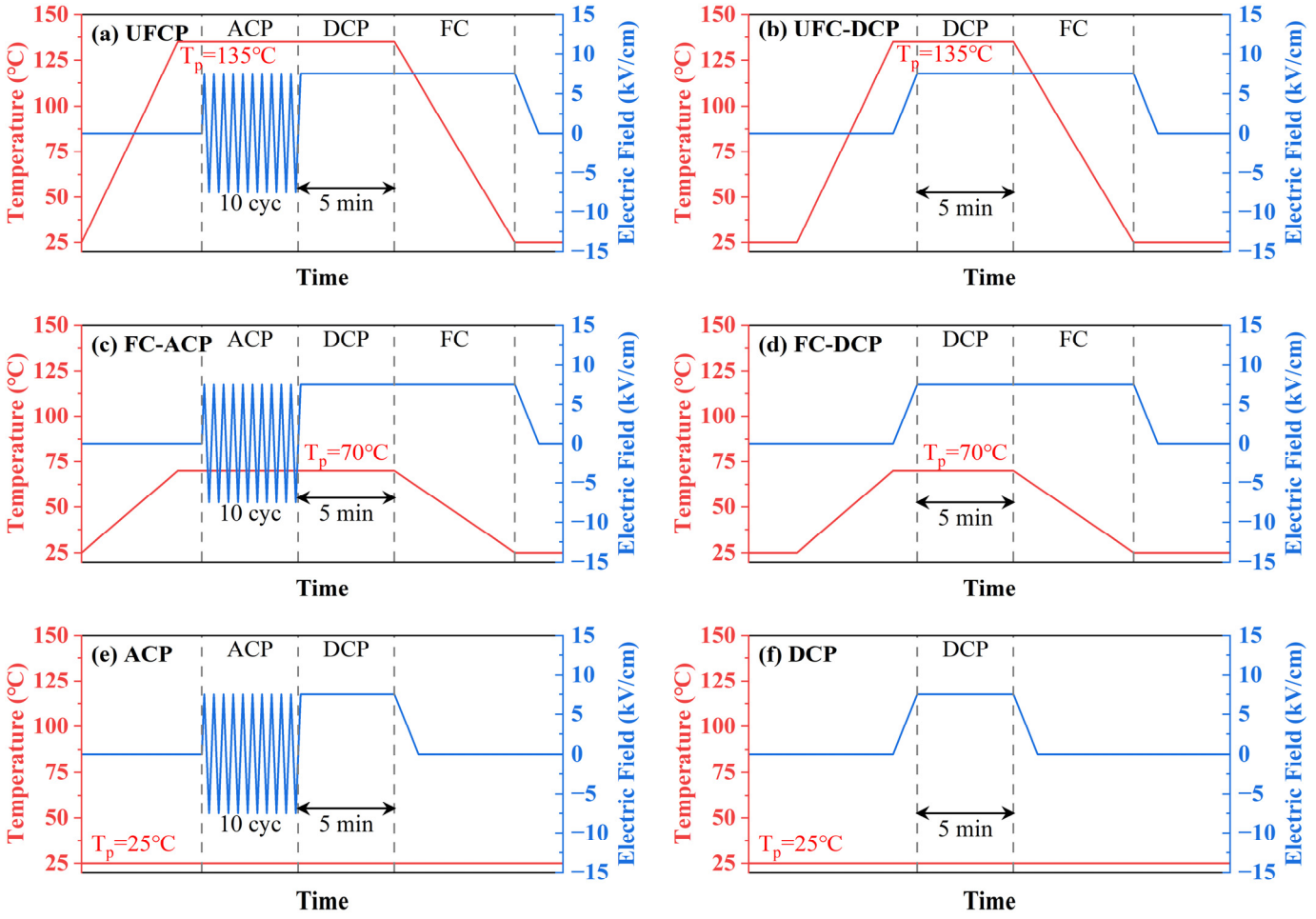

Figure 1. Schematic diagrams of (**a**) ultrahigh-temperature field-cooling polarization (UFCP), (**b**) ultrahigh-temperature field-cooling direct current polarization (UFC-DCP), (**c**) field-cooling alternating current polarization (FC-ACP), (**d**) field-cooling direct current polarization (FC-DCP), (**e**) room-temperature alternating current polarization (ACP), and (**f**) room-temperature direct current polarization (DCP) methods.

Here, ρ is the sample density, and l is the sample length. The mechanical quality factor Q_m was determined by using the 3dB bandwidth (Δf) of the resonance peak from the impedance spectrum, as expressed by

$$Q_m = \frac{f_r}{\Delta f} \quad (4)$$

To comprehensively evaluate the piezoelectric performance and energy conversion stability, the piezoelectric figure of merit ($FOM = d_{31} \times Q_m$) was introduced. This parameter was used to study the performance of the samples under high-power conditions.

A high-power characterization system was employed to characterize the piezoelectric performance of PMN-PT SCs under high-power conditions [41]. A function generator (Textronix AFG1022, Tektronix, Beaverton, OR, USA) produced a frequency-sweeping sinusoidal signal with constant peak voltage. The frequency sweep range was set from 30 kHz to 60 kHz, with a sweep time of 100 ms, to encompass the resonance and anti-resonance modes of the piezoelectric SCs. The sinusoidal signal was amplified to the desired voltage level by using a power amplifier (Aigtek ATA-3080, Aigtek, Xi'an, China)

and delivered to the sample through spring-loaded metal probes mounted on a fixture. Two probes were positioned at the center of the electrode areas to allow the sample to vibrate freely in the air. The vibration velocity along the longitudinal direction of the PMN-PT SCs was measured by using a vibrometer sensor (Polytec OFV-505, Polytec, Waldbronn, Germany). The voltage (V) across the sample was recorded by using an oscilloscope (Tektronix DPO 3054, Tektronix, Beaverton, OR, USA), and the current (I) flowing through the sample was captured with a current probe (Tektronix CT-1, Tektronix, Beaverton, OR, USA). The voltage, current, power, and vibration velocity of the samples in high-power characterization are shown in Figure A2, with the driving RMS voltage of the UFCP PMN-PT SCs set to 15 V as an example. The recorded signals were processed in MATLAB, where the impedance (Z) of the sample was calculated as $Z = V/I$. The impedance spectrum was obtained by performing a Fourier transform on the data. To ensure that the temperature of the samples remained unchanged during high-power characterization experiments, it was monitored by using an infrared thermal camera (FOTRIC 246 M, Fotric, Shanghai, China), as shown in Figure A3. Other relevant piezoelectric performance parameters were calculated following the same methodology as in the small-signal measurements, as described by Equations (1)–(4).

3. Results and Discussion

The performances of the PMN-PT samples with six different polarization methods under small-signal characterization conditions are presented in Figure 2. The data points represent the average of four samples, with error bars indicating variance.

The PMN-PT SCs polarized by the UFCP method demonstrate notably enhanced properties. The $\varepsilon_{33}^{T}/\varepsilon_0$ of the UFCP PMN-PT SCs reaches 7697, marking a 51.7% improvement compared with the 5075 obtained with the DCP method and 3.5% higher than the 7438 obtained with the ACP method. Moreover, the tanδ of UFCP PMN-PT is just 0.74%, representing a substantial reduction of 45.2% compared with the 1.35% observed in the ACP SCs. The higher tanδ of the ACP samples compared with the other literature data [42] may be due to the difference in electrode materials and polarization methods, as well as the effect of the thicker sample size in this study. This reduction is attributed to the elevated temperature conditions during UFCP, which lower E_c, facilitating polarization rotation at the reduced electric field and avoiding the defect proliferation caused by frequent domain structure flipping in the ACP method [24,25]. Regarding piezoelectric performance, the d_{33} of UFCP SCs reaches 2588 pC/N, 51.5% higher than the 1708 pC/N obtained with DCP and 4.5% greater than the 2476 pC/N obtained with ACP. Similarly, the d_{31} of UFCP SCs was 1126 pC/N, 68.6% higher than the 668 pC/N obtained with DCP and 44.0% greater than the 782 pC/N obtained with ACP. Additionally, the k_{31} for the UFCP samples reaches 0.559, representing a 40.1% improvement over DCP's 0.399 and a 49.1% increase compared with ACP's 0.375. Regarding Q_m, in the UFCP PMN-PT SCs, it is 105, outperforming DCP by 16.7% and ACP by 7.1%. The FOM reaches 119 nC/N for UFCP samples, representing a 98.3% increase over DCP and a 36.8% improvement compared with ACP. Overall, the PMN-PT SCs processed via UFCP demonstrated significantly enhanced dielectric and piezoelectric properties compared with those prepared by using the conventional DCP and ACP methods. These results underscore the potential of UFCP PMN-PT SCs to deliver higher signal output efficiency and stabler energy conversion performance, positioning them as a promising candidate for high-power applications.

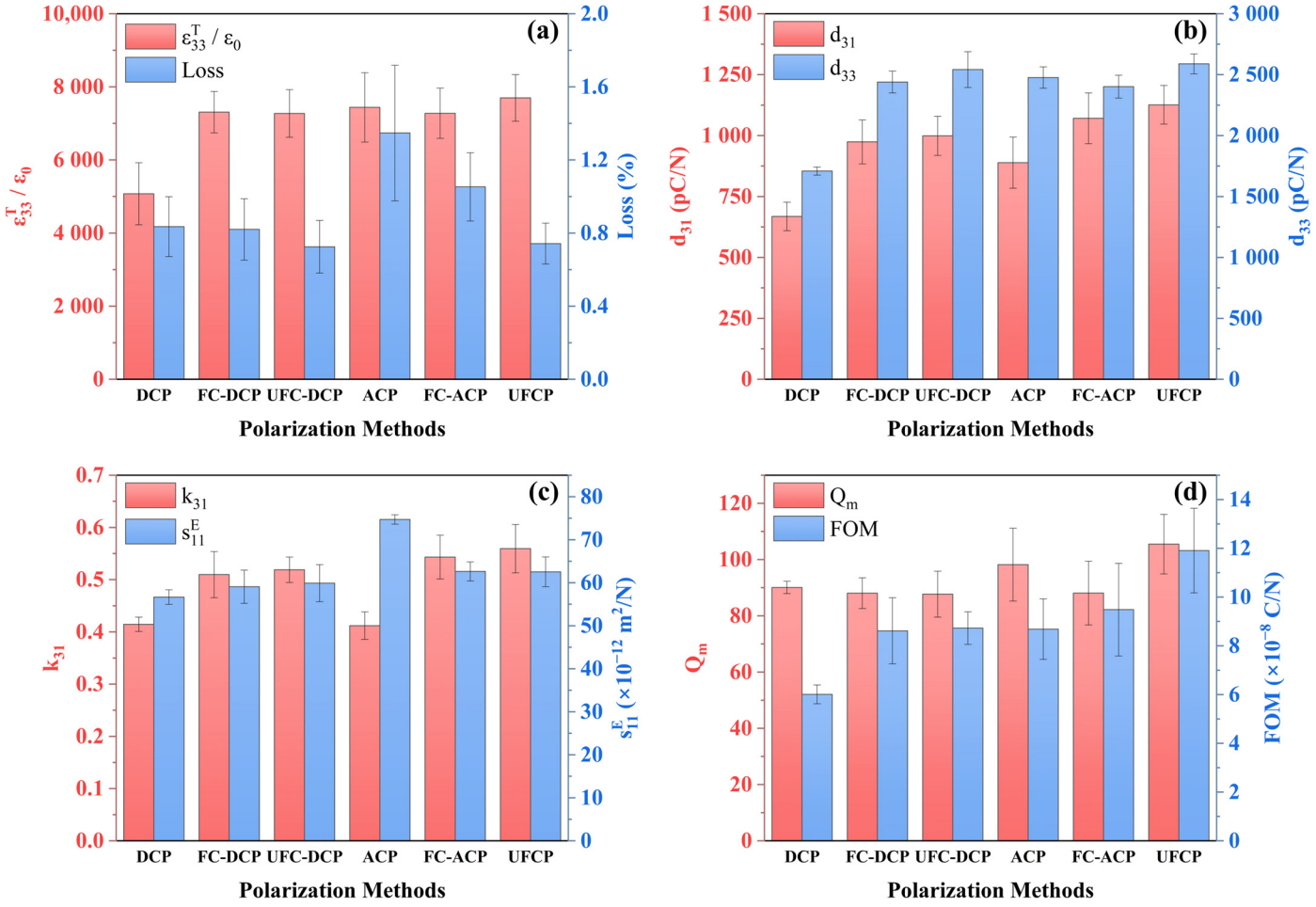

Figure 2. (**a**) Free dielectric constant $\varepsilon_{33}^T/\varepsilon_0$ and dielectric loss at 1 kHz, (**b**) piezoelectric constant d_{33} and d_{31}, (**c**) electromechanical coupling factor k_{31} and elastic compliance s_{11}^E, and (**d**) mechanical quality factor Q_m and piezoelectric figure of merit (FOM) as functions of different polarization methods in small-signal characterization.

The temperature dependence of the free dielectric constant $\varepsilon_{33}^T/\varepsilon_0$ for PMN-PT SCs treated with the DCP, ACP, and UFCP methods and the unpolarized state are illustrated in Figure 3. All the PMN-PT SCs exhibit a T_C of 130 ± 2 °C, marked by a pronounced peak in permittivity due to the phase transition from the T phase to the cubic (C) phase [43]. Below the Curie temperature, the PMN-PT SCs polarized by using the three methods display two distinct dielectric peaks observed at approximately 80 °C and 92 °C. These correspond to the phase transitions from the R phase to the M phase (T_{d1}) and from the M phase to the T phase (T_{d2}), respectively [21,29]. The T_{d1} of the DCP, ACP, and UFCP samples are 84 °C, 82 °C, and 78 °C, respectively, with the UFCP samples exhibiting the lowest transition temperature. These phase transitions confirm the coexistence of M and R phases within the PMN-PT SCs [18]. The enhanced electrical properties of PMN-PT SCs can be attributed to the forming of a low-symmetry multiphase structure and a refined domain configuration via phase transitions induced by the combined FCP procedures of dynamic ACP and DCP. For field-cooling ACP-DCP combined polarization below T_C, the T phase domains are established mainly prior to applying the AC electric field. Consequently, field-induced phase transitions are less likely to occur, resulting in the relaxation of defects under cyclic AC fields. This limitation could partially reduce the improvement in electrical performance compared with polarization at 135 °C. In contrast, the UFCP strategy optimizes the electrical performance of PMN-PT SCs. Leveraging a tailored polarization process above the Curie

temperature fosters superior dielectric and piezoelectric properties, making UFCP SCs highly advantageous for practical applications.

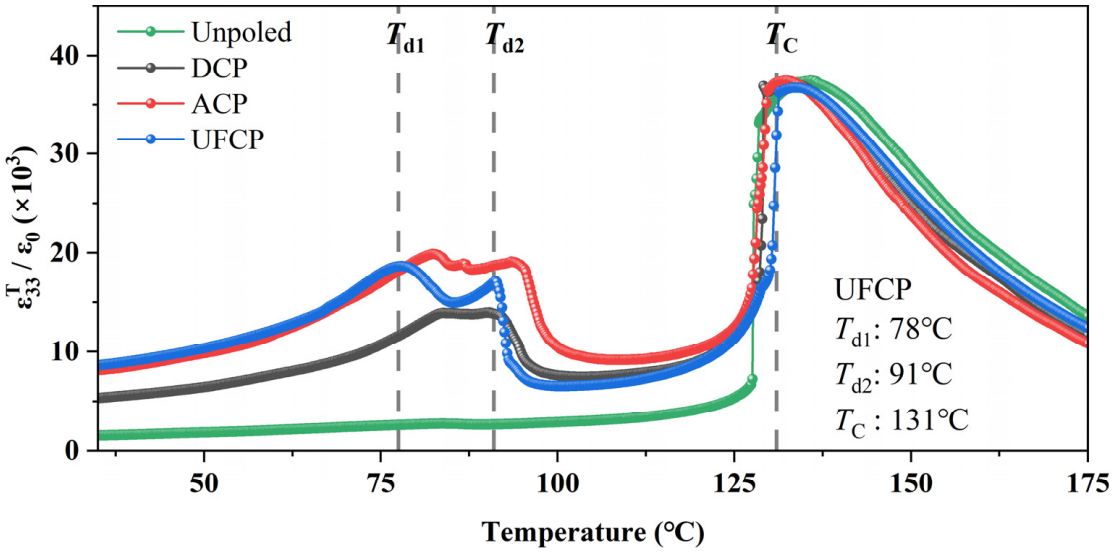

Figure 3. Temperature dependence of $\varepsilon_{33}^T/\varepsilon_0$ at 1 kHz of unpoled, DCP, ACP, and UFCP PMN-PT SCs.

Multiple polarization experiments were conducted at various temperatures to investigate the influence of field-cooling temperature on the piezoelectric properties during AC-DC combined polarization. The T_p range, spanning from RT (25 °C) to 155 °C, is categorized into three regions: RT region, field-cooling region 1 (FC-1), field-cooling region 2 (FC-2), and ultrahigh-temperature field-cooling region (UFC). The results are illustrated in Figure 4. The FC-1 region lies below T_{d1} and above RT, where no phase transitions occur during the polarization process. In contrast, the FC-2 region, situated between T_{d1} and T_C, undergoes phase transitions among the R phase, M phase, and T phase under polarization. Finally, the UFC region, positioned above T_C, induces partial transformation of the domain structure in PMN-PT SCs into the paraelectric cubic (C) phase.

As T_p increases from RT to 110 °C, the $\varepsilon_{33}^T/\varepsilon_0$ and d_{33} of the PMN-PT SCs decrease by approximately 8%. However, an improvement is observed in tanδ, which decreases from 1.35% to 0.68%, attributed to enhanced domain switching and accelerated domain wall movement at higher T_p [25]. When T_p reaches 110 °C, Q_m reaches the maximum of all temperatures, while d_{31} and k_{31} are relatively low. This phenomenon can be attributed to insufficient domain switching at this temperature. When T_p reaches slightly above T_C, improvements in k_{31} lead to a maximum d_{31} of 1126 pC/N and the highest FOM value. The highest k_{31} indicates that UFCP PMN-PT SCs achieve the utmost electromechanical conversion efficiency at this temperature. As T_p increases to 155 °C, the dielectric and piezoelectric properties exhibit a pronounced decline, approaching the levels observed under DC polarization alone at 135 °C. This decline suggests that the influence of the AC field on the domain structure diminishes at higher temperatures, likely due to insufficient field-induced phase transitions. Such transitions occur only within a narrow temperature range near T_C, where the required electric field strength is minimal. As T_p rises from T_C, the electric field necessary for inducing phase transitions increases significantly [44]. Therefore, PMN-PT SCs demonstrate vitally enhanced performance when subjected to multiphase transitions induced by AC fields during field cooling slightly above T_C, emphasizing the critical role of temperature in achieving optimal piezoelectric properties.

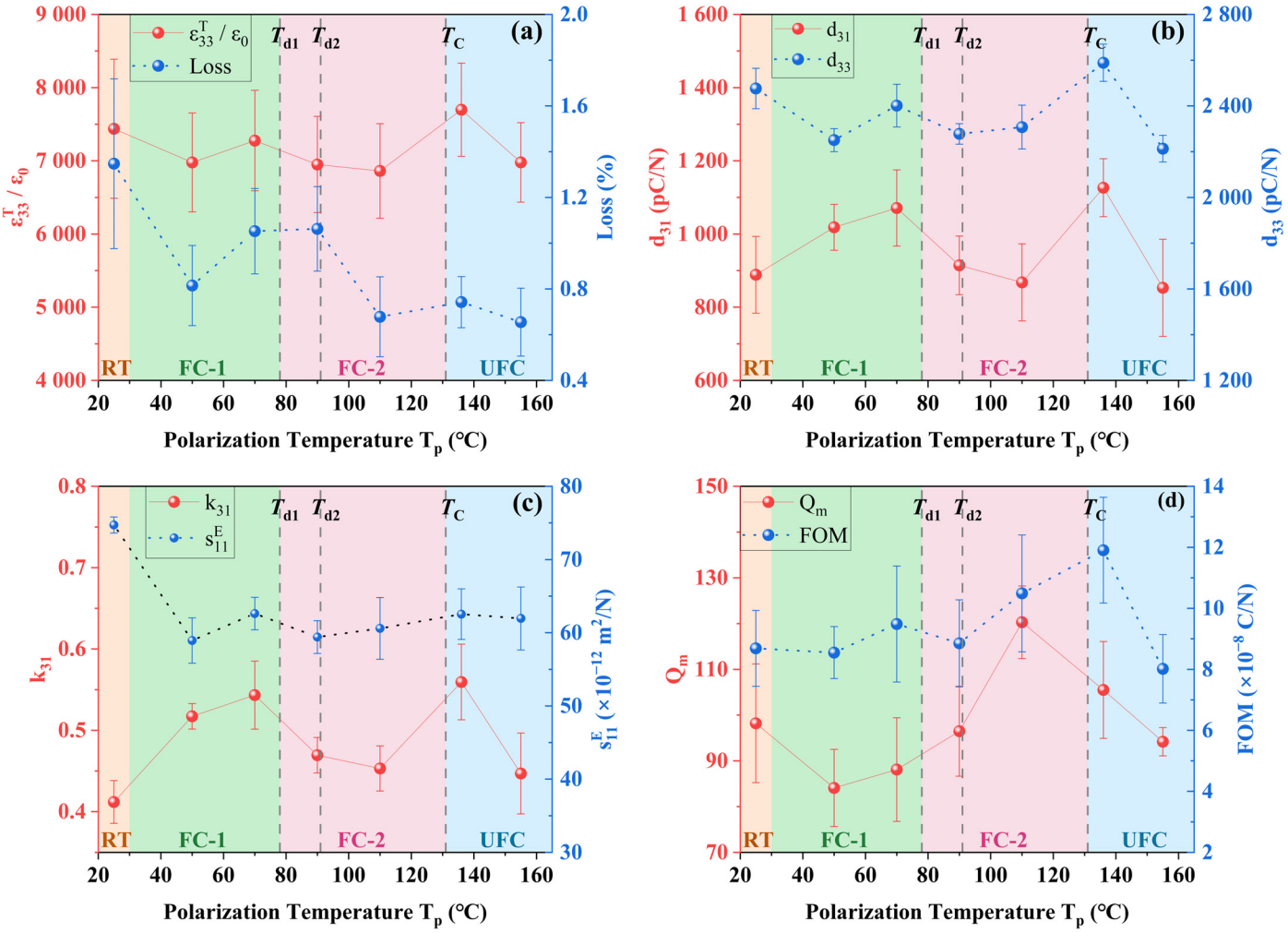

Figure 4. (**a**) $\varepsilon_{33}^{T}/\varepsilon_0$ and dielectric loss at 1 kHz, (**b**) d_{33} and d_{31}, (**c**) k_{31} and s_{11}^{E}, and (**d**) Q_m and FOM as functions of ACP PMN-PT SCs poled at different polarization temperatures T_p in small-signal characterization.

While UFCP PMN-PT SCs demonstrate superior d_{31} and Q_m under small-signal conditions, suggesting suitability for high-power piezoelectric applications, their performance characteristics under high-voltage excitation have yet to be thoroughly elucidated [35,37]. This study used a high-power piezoelectric performance characterization system to measure the impedance spectra of PMN-PT SCs polarized by three methods under root-mean-square (RMS) excitation voltages ranging from 1 V to 15 V. The trends in various performance parameters with the increase in voltage were also investigated. As shown in Figure 5, with the increase in excitation voltage, the resonance and anti-resonance peaks of the impedance spectra shifted progressively to lower frequencies. The resonance peaks shifted more than the anti-resonance peaks for all three polarization methods. For instance, for the UFCP PMN-PT SCs, the f_r decreased from 43.2 kHz at 1 V to 40.9 kHz at 15 V, while f_a decreased from 48.4 kHz to 47.8 kHz. Additionally, the resonance impedance increased, and the anti-resonance impedance decreased with the increase in voltage. For the UFCP PMN-PT SCs, the resonance impedance increased from 31.8 Ω to 110.6 Ω, while the anti-resonance impedance decreased from 20.9 kΩ to 7.9 kΩ. These results underline the voltage-dependent behavior of piezoelectric parameters under high-power conditions, emphasizing the importance of considering such nonlinear effects in designing and applying high-power piezoelectric devices.

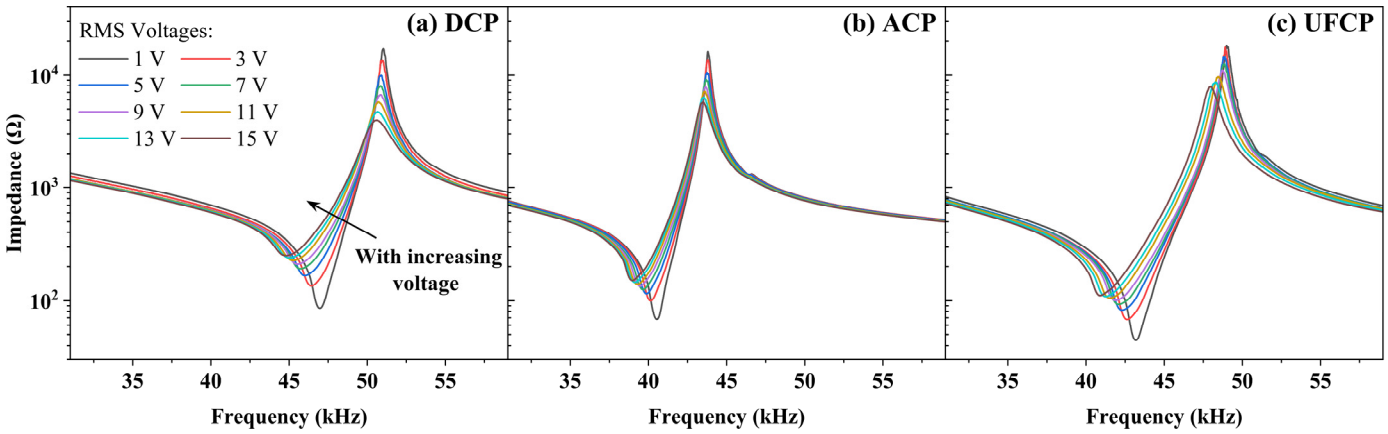

Figure 5. Impedance spectra as functions of frequency under different root-mean-square (RMS) driving voltages for (**a**) DCP, (**b**) ACP, and (**c**) UFCP PMN-PT SCs.

As the amplitude of the AC driving voltage increases, the performance parameters of the PMN-PT SCs exhibit significant changes, following similar trends across samples treated with the DCP, ACP, and UFCP methods, as illustrated in Figure 6. As depicted in Figure A3b, the temperatures of the three samples were maintained constant throughout the high-power testing experiments. Consequently, the observed variations in all parameters were independent of temperature. In UFCP PMN-PT SCs, d_{31} increased from 1011 pC/N at 1 V to 1184 pC/N at 15 V, representing a 17.1% improvement. k_{31} rose from 0.503 to 0.558, marking a 10.9% increase. However, Q_m decreased to just 28.8 at 15 V, leading to a decline in the piezoelectric FOM to 3.41×10^{-8} C/N. Comparing the high-power performance of PMN-PT SCs with different polarization methods reveals distinctive trends. As the voltage increases, the relative advantage of UFCP crystals in terms of d_{31} over DCP samples narrows from 44.0% to 31.8%, while its advantage over ACP samples decreases from 24.6% to 10.6%. For Q_m, the advantage of UFCP over DCP widens from 45.0% to 74.8%, though its superiority over ACP shrinks from 35.8% to 30.3%. Furthermore, at the same driving voltage, the UFCP PMN-PT SCs achieve a resonance power output of 5.04 W, 4.43 times that with DCP and 2.72 times that with ACP. This superior power output is attributed to the highest k_{31} among the three methods, enabling the UFCP samples to achieve greater mechanical energy output at equivalent voltage levels, demonstrating exceptional energy conversion capabilities. The UFCP samples exhibit consistently higher vibration velocities compared with the DCP and ACP samples. At an RMS driving voltage of 11 V, the vibration velocity of the UFCP samples reaches 509 mm/s. However, as the voltage increases further, the growth rate of the vibration velocity slows significantly, a behavior not observed in the DCP or ACP samples. This indicates that the vibration velocity of the UFCP samples is nearing its structural and performance limitations. Overall, the FOM of the UFCP PMN-PT SCs is 130.5% higher than that obtained with DCP and 44.1% higher than that obtained with ACP, even under high-power AC driving conditions at 15 V. These results highlight the UFCP method's ability to deliver higher signal output and superior energy conversion efficiency in practical high-power applications.

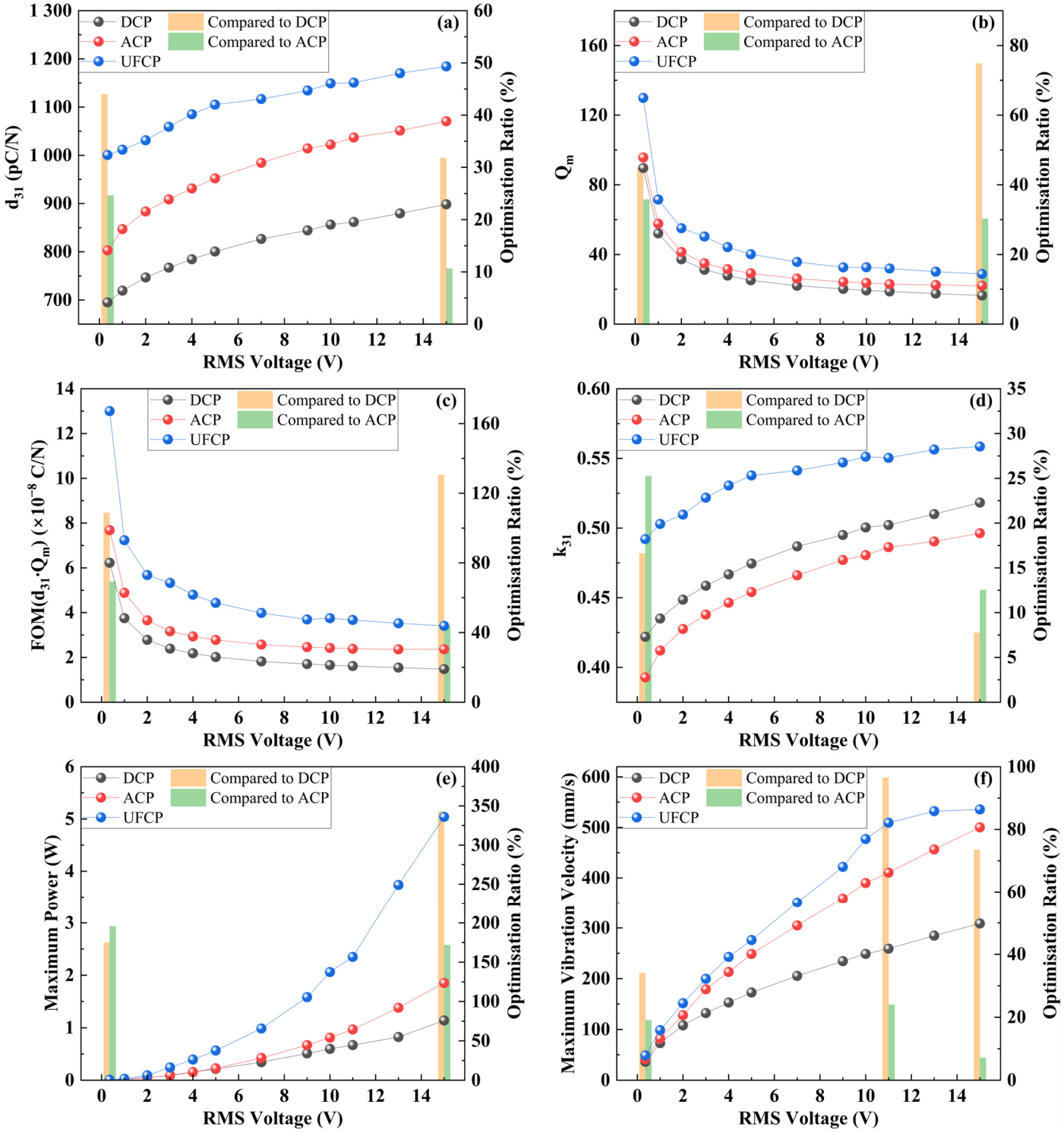

Figure 6. (**a**) d_{31}, (**b**) Q_m, (**c**) FOM, (**d**) k_{31}, (**e**) maximum power at resonant frequency, and (**f**) maximum vibration velocity at resonant frequency as functions of RMS driving voltage in high-power characterization.

4. Conclusions

This study introduces a new UFCP technique, which combines DC and AC polarization above T_C, applied to MPB-region PMN-PT SCs. Under small-signal characterization, the UFCP method enhances material performance, achieving a d_{31} of 1126 pC/N and a k_{31} of 0.559. The UFCP method substantially outperforms traditional DCP, increasing d_{31} by 68.6%, Q_m by 16.7%, and the FOM by 98.3%. Under high-power excitation with an RMS

voltage at 15 V, it achieves a staggering 343% increase in power and a 130.5% improvement in the FOM compared with DCP. Similarly, UFCP demonstrates notable advantages over the ACP approach at RT, with increases of 44.0% in d_{31}, 7.1% in Q_m, and 36.8% in the FOM, showing its exceptional utility in power piezoelectric devices. The analysis of dielectric spectra offers critical insights into the underlying mechanisms responsible for the observed performance enhancements. The UFCP approach promotes electric field-induced phase transitions at T_C, resulting in a stable, low-symmetry multiphase domain configuration. This structural modification significantly improves the electrical properties of PMN-PT SCs. In summary, the UFCP method presents a promising pathway for optimizing high-power piezoelectric devices, paving the way for applications across multiple fields requiring high-performance piezoelectric materials.

Author Contributions: Conceptualization, Y.Z.; Data curation, Y.Z.; Formal analysis, X.W. (Xiaobo Wang) and W.X.; Funding acquisition, C.L.; Methodology, Y.Z., X.W. (Xiaobo Wang) and C.L.; Project administration, C.L.; Resources, C.L.; Software, X.W. (Xinran Wen); Supervision, C.L.; Validation, Y.Z. and X.W. (Xiaobo Wang); Writing—original draft, Y.Z.; Writing—review and editing, C.L. All authors have read and agreed to the published version of the manuscript.

Funding: This research was funded by National Natural Science Foundation of China (grant No. 12104300) and National Key R&D Program of China (grant No. 2021YFA0716502).

Data Availability Statement: The original contributions presented in the study are included in the article, and further inquiries can be directed to the corresponding authors.

Conflicts of Interest: The authors declare no conflicts of interest.

Abbreviations

PMN-PT	$Pb(Mg_{1/3}Nb_{2/3})O_3$-$PbTiO_3$
PIN-PMN-PT	$Pb(In_{1/2}Nb_{1/2})O_3$-$Pb(Mg_{1/3}Nb_{2/3})O_3$-$PbTiO_3$
PZT	$Pb(Zr_{1-x}Ti_x)O_3$
PT	$PbTiO_3$
SCs	single crystals
AC	alternating current
ACP	alternating current polarization
DC	direct current
DCP	direct current polarization
FC	field cooling
FCP	field-cooling polarization
UFC	ultrahigh-temperature field cooling
UFCP	ultrahigh-temperature field-cooling polarization
FOM	piezoelectric figure of merit
MEMSs	micro-electromechanical systems
MPB	morphotropic phase boundary
RT	room temperature
R	rhombohedral
T	tetragonal
C	cubic
M	monoclinic
RMS	root mean square
FWHM	full width at half maximum

Appendix A

Figure A1 presents the impedance spectra as functions of frequency for PMN-PT SCs subjected to three different polarization methods obtained through small-signal character-

ization both before and after high-power experiments. The results demonstrate that the resonance and anti-resonance frequencies, as well as the overall impedance spectral profiles, remain virtually unchanged before and after high-power characterization. This consistency in impedance spectra indicates that the polarization state of the PMN-PT SCs was not affected by the high-power characterization experiments. Consequently, the stability of the polarization state ensures the reliability of the high-power performance data reported in this study.

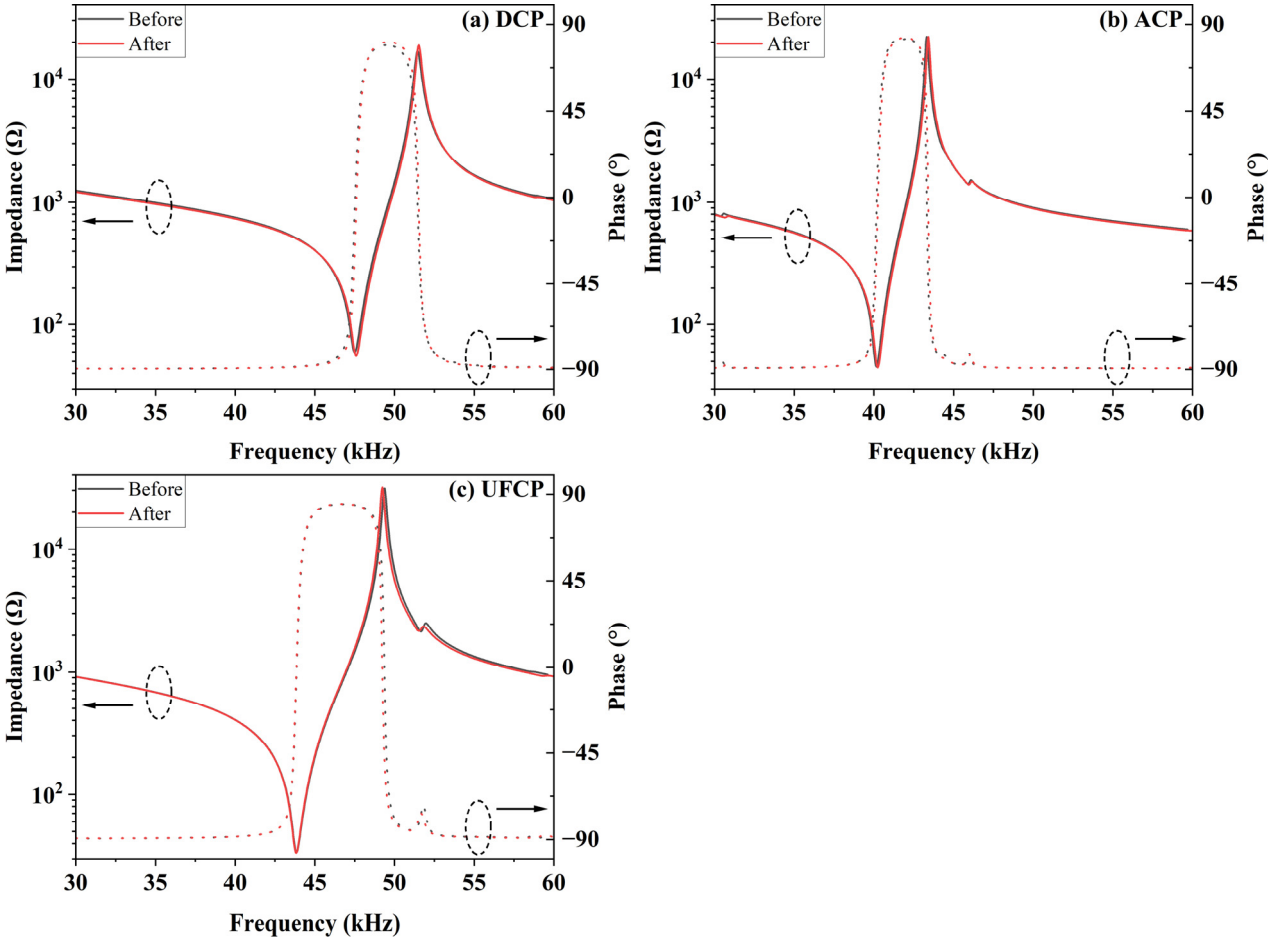

Figure A1. Impedance spectra as functions of frequency before and after high-power characterization experiments for (**a**) DCP, (**b**) ACP, and (**c**) UFCP PMN-PT SCs in small-signal characterization.

Figure A2 illustrates the high-power characterization of the samples, displaying their voltage, current, power, and vibration velocity, exemplified by a driving RMS voltage of 15 V for the UFCP PMN-PT SCs. During the characterization process, a constant voltage amplitude was maintained while the frequency was swept from 30 kHz to 60 kHz within a controlled sweep time of 100 ms. Although heat is generated during high-power testing, the extremely short testing duration prevents heat accumulation and the resultant increase in sample temperature, thereby eliminating the potential influence of temperature fluctuations on the sample parameters. The variation in current during the characterization is depicted in Figure A2b, where the current attains its maximum value at the resonant frequency and reaches its minimum at the anti-resonant frequency. The power of the PMN-PT sample, as shown in Figure A2c, was calculated by using the formula $P = I \times V$. The sample power peaked at 5.04 W when the frequency corresponded to the resonant frequency, with a full width at half maximum (FWHM) of the power curve being 5.5 ms. This narrow FWHM ensures that sample testing can be completed in an extremely short duration, remaining

unaffected by thermal effects. Similarly, the vibration velocity of the sample, illustrated in Figure A2d, achieved its maximum value of 535 mm/s at the resonant frequency.

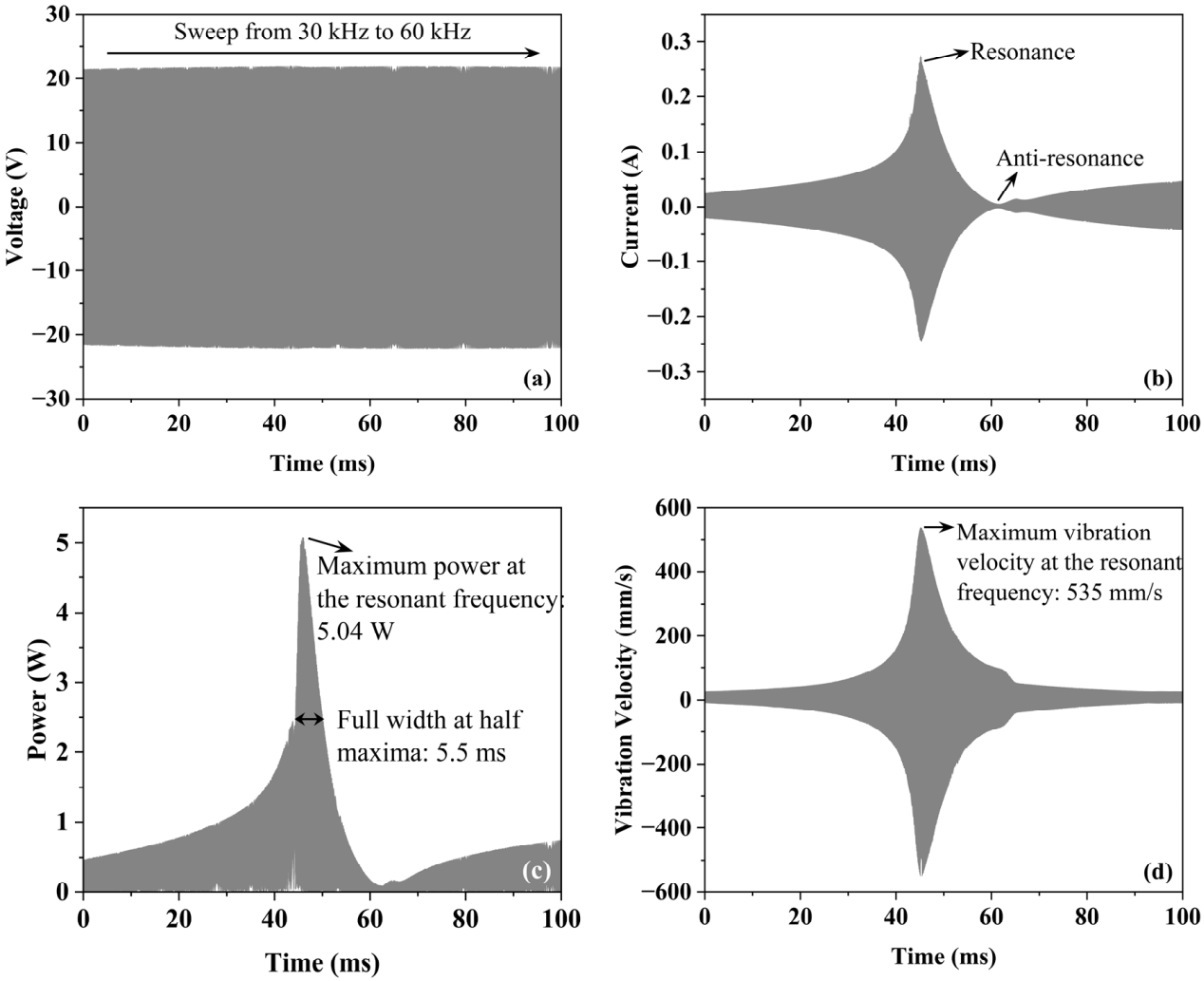

Figure A2. (**a**) Voltage, (**b**) current, (**c**) power, and (**d**) vibration velocity of UFCP PMN-PT SC during high-power characterization experiments, with driving RMS voltage set to 15 V as an example.

Figure A3a illustrates the infrared thermal imaging of UFCP PMN-PT SCs under a driving RMS voltage of 15 V. Owing to the low emissivity of metallic materials, it was not feasible to measure the temperature of the silver-paste electrodes by directly using the infrared camera. Therefore, the highest temperature on the sample's side surface (marked by the white rectangular region) was recorded as the representative peak temperature during high-power experiments. Figure A3b displays the relationship between the maximum temperature of PMN-PT SCs and the RMS driving voltage applied during the experiments. The results indicate that the recorded temperatures remained stable within the range of 19 °C to 21 °C. These observations substantiate that the high-power characterization process did not induce a significant temperature increase, confirming that the observed parameter changes were independent of thermal effects.

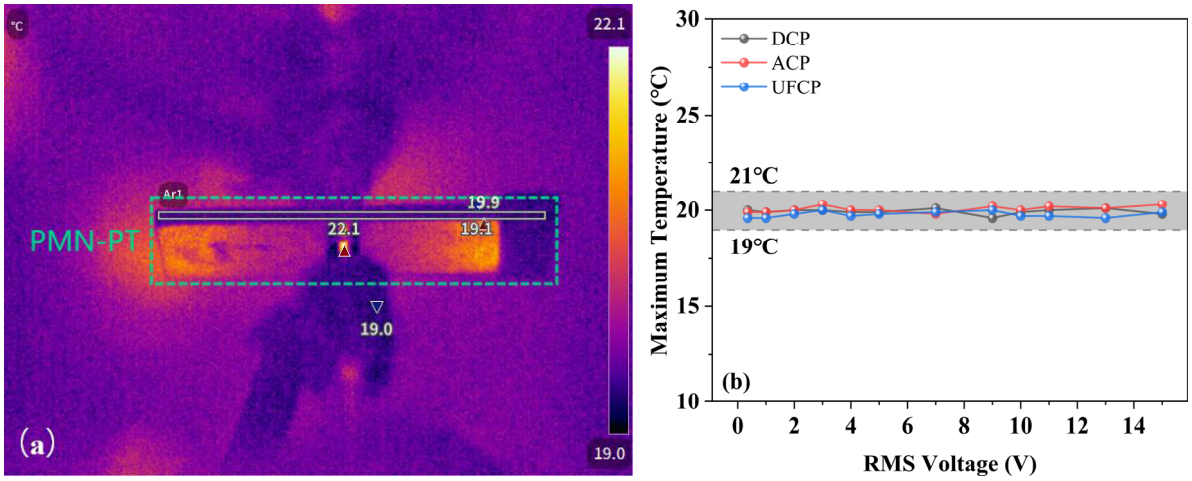

Figure A3. Monitoring temperature of PMN-PT SCs during high-power experiments using an infrared thermal camera. (**a**) Infrared thermography of UFCP PMN-PT SC with driving RMS voltage set to 15 V. (**b**) Maximum temperature of PMN-PT SCs as a function of RMS driving voltage in high-power characterization.

References

1. Zhou, S.; Gao, X.; Park, G.; Yang, X.; Qi, B.; Lin, M.; Huang, H.; Bian, Y.; Hu, H.; Chen, X.; et al. Transcranial volumetric imaging using a conformal ultrasound patch. *Nature* **2024**, *629*, 810–818. [CrossRef] [PubMed]
2. Qin, S.Y.; Chen, J.Q.; Yang, P.; Liu, Z.Q.; Tao, X.L.; Dong, X.Y.; Hu, J.; Chu, X.C.; Wang, Z.L.; Chen, X.Y. A Piezo-Tribovoltaic Nanogenerator with Ultrahigh Output Power Density and Dynamic Sensory Functions. *Adv. Energy Mater.* **2024**, *14*, 2303080. [CrossRef]
3. Song, Y.; Tang, Z.K.; Shi, R.C.; Wang, S.J.; Lin, D.; Luo, C.T. Design of PMN-PT-based dual-resonance acoustic emission sensor for partial discharge detection. *Sens. Actuators A-Phys.* **2024**, *373*, 115432. [CrossRef]
4. Wang, X.; Zhang, R.; Zhu, Y.; Luo, B.; Luo, C.; Han, T. A Piezoelectric-Piezoresistive Coupled Electric Field Sensor for Large Dynamic Range Measurement from DC to 1.5 kHz. *IEEE Sens. J.* **2024**, *24*, 902. [CrossRef]
5. Zheng, G.B.; Chen, Z.J.; Chen, X.; Liu, S.Q.; Cao, W.W. High-field complex parameters characterization of PMN-PT single crystal/epoxy 1-3 composites (φ = 0.4) under a high AC electric field with a varied intensity. *Ultrasonics* **2024**, *144*, 107447. [CrossRef]
6. Li, J.; Torelló, A.; Kovacova, V.; Prah, U.; Aravindhan, A.; Granzow, T.; Usui, T.; Hirose, S.; Defay, E. High cooling performance in a double-loop electrocaloric heat pump. *Science* **2023**, *382*, 801–805. [CrossRef]
7. Wu, J.; Wu, L.J.; Song, R.; Niu, J.Y.; Xie, M.L.; Cao, M.Y.; Zhang, Q.; Liu, Y.X.; Li, Y.B. A Two-DOF Linear Ultrasonic Motor with High Thrust Force Density and High Power Density Utilizing Torsional/Centrosymmetric-Bending/Symmetric-Bending Modes. *IEEE Trans. Ind. Electron.* **2022**, *69*, 8220–8230. [CrossRef]
8. Yang, L.Y.; Huang, H.B.; Xi, Z.Z.; Zheng, L.M.; Xu, S.Q.; Tian, G.; Zhai, Y.Z.; Guo, F.F.; Kong, L.P.; Wang, Y.G.; et al. Simultaneously achieving giant piezoelectricity and record coercive field enhancement in relaxor-based ferroelectric crystals. *Nat. Commun.* **2022**, *13*, 2444. [CrossRef]
9. Tang, W.B.; Wang, Y.Q.; Xiang, G.L.; Zhao, X.F.; Pan, Z.Y.; Wang, Y.P.; Yang, Y.; Wang, Y.J.; Yuan, G.L. Enhanced high-power performance of Fe-doped PZMNZT piezoelectric ceramics. *J. Am. Ceram. Soc.* **2023**, *106*, 6868–6878. [CrossRef]
10. Kong, S.Y.; Hong, C.H.; Zhang, W.J.; Liu, Y.; Wang, Z.J.; Yang, X.M.; Su, R.B.; Long, X.F.; He, C. Performance enhancement of soft-PZT5 piezoelectric ceramics using poling technique. *J. Am. Ceram. Soc.* **2022**, *105*, 4744–4750. [CrossRef]
11. Kuwata, J.; Uchino, K.; Nomura, S. Dielectric and Piezoelectric Properties of 0.91Pb($Zn_{1/3}Nb_{2/3}$)O_3-0.09$PbTiO_3$ Single Crystals. *Jpn. J. Appl. Phys.* **1982**, *21*, 1298. [CrossRef]
12. Kuwata, J.; Uchino, K.; Nomura, S. Phase transitions in the Pb ($Zn_{1/3}Nb_{2/3}$)O_3-$PbTiO_3$ system. *Ferroelectrics* **1981**, *37*, 579–582. [CrossRef]
13. Shrout, T.R.; Chang, Z.P.; Kim, N.; Markgraf, S. Dielectric behavior of single crystals near the (1−X) Pb($Mg_{1/3}Nb_{2/3}$)O_3-(x) $PbTiO_3$ morphotropic phase boundary. *Ferroelectr. Lett. Sect.* **1990**, *12*, 63–69. [CrossRef]
14. Chen, Y.-H.; Uchino, K.; Viehland, D. Substituent Effects in 0.65Pb($Mg_{1/3}Nb_{2/3}O_{30.35}$$PbTiO_3$ Piezoelectric Ceramics. *J. Electroceram.* **2001**, *6*, 13–19. [CrossRef]
15. Sun, E.W.; Cao, W.W. Relaxor-based ferroelectric single crystals: Growth, domain engineering, characterization and applications. *Prog. Mater. Sci.* **2014**, *65*, 124–210. [CrossRef]

16. Hu, M.; Chang, Z.C.; Nie, N.; Wan, Z.J.; Dong, W.; Fu, Q.Y. La-doped PMN-PT transparent ceramics with ultra-high electro-optic effect and its application in optical devices. *J. Adv. Ceram.* **2023**, *12*, 1441–1453. [CrossRef]
17. Negi, A.; Kim, H.P.; Hua, Z.L.; Timofeeva, A.; Zhang, X.Y.; Zhu, Y.; Peters, K.; Kumah, D.; Jiang, X.N.; Liu, J. Ferroelectric Domain Wall Engineering Enables Thermal Modulation in PMN-PT Single Crystals. *Adv. Mater.* **2023**, *35*, 2211286. [CrossRef]
18. Kim, H.P.; Wan, H.; Luo, C.; Sun, Y.; Yamashita, Y.; Karaki, T.; Lee, H.Y.; Jiang, X. A Review on Alternating Current Poling for Perovskite Relaxor-$PbTiO_3$ Single Crystals. *IEEE Trans. Ultrason. Ferroelectr. Freq. Control* **2022**, *69*, 3037–3047. [CrossRef]
19. Yamamoto, N.; Yamashita, Y.; Hosono, Y.; Itsumi, K.; Higuchi, K. Ultrasonic Probe, Piezoelectric Transducer, Method of Manufacturing Ultrasonic Probe, and Method of Manufacturing Piezoelectric Transducer. U.S. Patent No. US 2014/0062261 A1, 6 March 2014.
20. Guo, L.; Su, B.; Wang, C.X.; He, X.; Wang, Z.J.; Yang, X.M.; Long, X.F.; He, C. Orientation dependence of dielectric and piezoelectric properties of tetragonal relaxor ferroelectric single crystals by alternate current poling. *J. Appl. Phys.* **2020**, *127*, 184104. [CrossRef]
21. Wang, S.; Liu, Z.; Han, L.; Yang, X.; Zhang, X.; Li, X.; Liu, L.; Karpinsky, D.; Lookman, T.; Luo, H.; et al. Mesophase induced by alternating-current poling in relaxor ferroelectric single crystals. *Acta Mater.* **2024**, *268*, 119782. [CrossRef]
22. Wu, H.; Han, S.; Liu, J.; Zhu, X.; Wang, J.; Sha, H.; Xu, G. Enhanced high-power behaviors of Mn-doped $Pb(In_{1/2}Nb_{1/2})O_3$-Pb(Mg1/3Nb2/3)O_3-$PbTiO_3$ piezoelectric crystals through combining direct and alternating current polarization. *J. Alloys Compd.* **2024**, *989*, 174370. [CrossRef]
23. Wan, H. Study on Alternating Current Poling of Relaxor-$PbTiO_3$ Single Crystals. Ph.D. Thesis, North Carolina State University, Raleigh, NC, USA, 2022.
24. Sun, Y.Q.; Karaki, T.; Fujii, T.; Yamashita, Y. Enhanced electric property of relaxor ferroelectric crystals with low AC voltage high-temperature poling. *Jpn. J. Appl. Phys.* **2020**, *59*, SPPD08. [CrossRef]
25. Luo, C.; Karaki, T.; Yamashita, Y.; Xu, J.Y. High temperature and low voltage AC poling for $0.24Pb(_{1/2}Nb_{1/2})O$-$0.46Pb(Mg_{1/3}Nb_{2/3})O_3$-$0.30PbTiO_3$ piezoelectric single crystals manufactured by continuous-feeding Bridgman method. *J. Mater.* **2021**, *7*, 621–628. [CrossRef]
26. Xiong, J.J.; Wang, Z.J.; Yang, X.M.; Long, X.F.; He, C. Optimizing the Piezoelectric and Dielectric Properties of $Pb(In_{1/2}Nb_{1/2})O$-3-$PbTiO_3$ Ferroelectric Crystals via Alternating Current Poling Waveform. *IEEE Trans. Ultrason. Ferroelectr. Freq. Control* **2021**, *68*, 2775–2780. [CrossRef]
27. Qiu, C.R.; Wang, B.; Zhang, N.; Zhang, S.J.; Liu, J.F.; Walker, D.; Wang, Y.; Tian, H.; Shrout, T.R.; Xu, Z.; et al. Transparent ferroelectric crystals with ultrahigh piezoelectricity. *Nature* **2020**, *577*, 350–354. [CrossRef]
28. Yamashita, Y.; Yamagata, Y.; Xiang, Y.; Maiwa, H.; Xu, Z.Z.; Jiang, X.N. Comparison of field-cooling DC poling and AC poling for lead perovskite relaxor-$PbTiO_3$ single crystals grown by a continuous feeding Bridgman process. *Jpn. J. Appl. Phys.* **2024**, *63*, 04SP37. [CrossRef]
29. Luo, C.; Karaki, T.; Wang, Z.K.; Sun, Y.Q.; Yamashita, Y.; Xu, J.Y. High piezoelectricity after field cooling AC poling in temperature stable ternary single crystals manufactured by continuous-feeding Bridgman method. *J. Adv. Ceram.* **2022**, *11*, 57–65. [CrossRef]
30. Shibiru, A.T.; Fujii, I.; Nam, H.; Sapkota, P.; Khanal, G.P.; Wang, Z.K.; Ueno, S.; Wada, S. Optimization of conditions for AC plus DC poling above Curie temperature of barium titanate ceramic for piezoelectric property enhancement. *J. Ceram. Soc. Jpn.* **2024**, *132*, 346–349. [CrossRef]
31. Shibiru, A.T.; Fujii, I.; Sapkota, P.; Nam, H.; Khanal, G.P.; Ueno, S.; Wada, S. Advancing piezoelectric properties of barium titanate ceramic through AC plus DC field poling over Curie temperature. *Jpn. J. Appl. Phys.* **2024**, *63*, 08SP10. [CrossRef]
32. Chen, Z.J.; Song, L.J.; Cao, W.W. Characterization of high-power mechanical quality factor of piezoelectric ceramic discs under self-heating condition. *J. Mater. Res. Technol.* **2023**, *23*, 5040–5049. [CrossRef]
33. Song, H.C.; Kim, S.W.; Kim, H.S.; Lee, D.G.; Kang, C.Y.; Nahm, S. Piezoelectric Energy Harvesting Design Principles for Materials and Structures: Material Figure-of-Merit and Self-Resonance Tuning. *Adv. Mater.* **2020**, *32*, 2002208. [CrossRef] [PubMed]
34. Adoukatl, C.; Ntamack, G.E.; Azrar, L. High order analysis of a nonlinear piezoelectric energy harvesting of a piezo patched cantilever beam under parametric and direct excitations. *Mech. Adv. Mater. Struct.* **2023**, *30*, 4835–4861. [CrossRef]
35. Yu, J.W.; Xu, L. Nonlinear Equivalent Circuit of High-Power Sandwich Piezoelectric Ultrasonic Transducer. *IEEE Trans. Ultrason. Ferroelectr. Freq. Control* **2022**, *69*, 3126–3136. [CrossRef]
36. Li, G.; Tian, F.H.; Gao, X.Y.; Tian, H.; Qiao, L.; Liu, J.F.; Li, F.; Xu, Z. Investigation of High-Power Properties of PIN-PMN-PT Relaxor-Based Ferroelectric Single Crystals and PZT-4 Piezoelectric Ceramics. *IEEE Trans. Ultrason. Ferroelectr. Freq. Control* **2020**, *67*, 1641–1646. [CrossRef]
37. Luan, P.; Liu, X.; Du, H.L.; Wu, W.H.; Hu, H.L.; Li, F.; Wei, X.Y.; Xu, Z. High second-order nonlinearity in single-domain tetragonal PMN-PT single crystal. *Appl. Phys. Lett.* **2024**, *125*, 042901. [CrossRef]
38. Xu, G.S.; Luo, H.S.; Guo, Y.P.; Gao, Y.Q.; Xu, H.Q.; Qi, Z.Y.; Zhong, W.Z.; Yin, Z.W. Growth and piezoelectric properties of $Pb(Mg_{1/3}Nb_{2/3})O_3$-$PbTiO_3$ crystals by the modified Bridgman technique. *Solid State Commun.* **2001**, *120*, 321–324. [CrossRef]
39. *IEEE Std 1859-2017*; IEEE Standard for Relaxor-Based Single Crystals for Transducer and Actuator Applications. IEEE: New York, NY, USA, 2017. [CrossRef]

40. *IEEE Std 176-1987*; IEEE Standard on Piezoelectricity. IEEE: New York, NY, USA, 1988. [CrossRef]
41. Xue, W.; Wang, X.; Zhu, Y.; Luo, C. Studies on the High-Power Piezoelectric Property Measurement Methods and Decoupling the Power and Temperature Effects on PZT-5H. *Sensors* **2025**, *25*, 349. [CrossRef]
42. Sun, Y.Q.; Karaki, T.; Fujii, T.; Yamashita, Y.J. Spurious-mode vibrations caused by alternating current poling and their solution process for $Pb(Mg_{1/3}Nb_{2/3})O$-3-$PbTiO_3$ single crystals. *J. Mater.* **2022**, *8*, 96–103. [CrossRef]
43. Kim, H.P.; Wan, H.; Lee, H.Y.; Yamashita, Y.; Jo, W.; Jiang, X. Thermal stability studies of alternating current poled $Pb(Mg_{1/3}Nb_{2/3})O_3$-$PbTiO_3$ single crystals grown by solid-state crystal growth. *Mater. Res. Lett.* **2023**, *11*, 383–390. [CrossRef]
44. Wang, Z.K.; Fujii, I.; Saito, S.; Nam, H.; Shibiru, A.T.; Ueno, S.; Wada, S. Enhanced piezoelectric properties of ⟨110⟩ grain-oriented 0.50(BiNa)TiO-0.50BaTiO ceramics by domain engineering above Curie temperature. *J. Ceram. Soc. Jpn.* **2024**, *132*, 350–357. [CrossRef]